

# Monte Carlo Glauber wounded nucleon model with meson cloud

B.G. Zakharov<sup>1</sup>

<sup>1</sup>*L.D. Landau Institute for Theoretical Physics, GSP-1, 117940, Kosygina Str. 2, 117334 Moscow, Russia*  
(Dated: November 18, 2016)

We study the effect of the nucleon meson cloud on predictions of the Monte Carlo Glauber wounded nucleon model for  $AA$ ,  $pA$ , and  $pp$  collisions. From the analysis of the data on the charged multiplicity density in  $AA$  collisions we find that the meson-baryon Fock component reduces the required fraction of binary collisions by a factor of  $\sim 2$  for Au+Au collisions at  $\sqrt{s} = 0.2$  TeV and  $\sim 1.5$  for Pb+Pb collisions at  $\sqrt{s} = 2.76$  TeV. For central  $AA$  collisions the meson cloud can increase the multiplicity density by  $\sim 16 - 18\%$ . We give predictions for the midrapidity charged multiplicity density in Pb+Pb collisions at  $\sqrt{s} = 5.02$  TeV for the future LHC run 2. We find that the meson cloud has a weak effect on the centrality dependence of the ellipticity  $\epsilon_2$  in  $AA$  collisions. For collisions of the deformed uranium nuclei at  $\sqrt{s} = 0.2$  TeV we find that the meson cloud may improve somewhat agreement with the data on the dependence of the elliptic flow on the charged multiplicity for very small centralities defined via the ZDCs signals. We find that the meson cloud may lead to a noticeable reduction of  $\epsilon_2$  and the size of the fireball in  $pA$  and  $pp$  collisions.

PACS numbers:

## I. INTRODUCTION

Experiments at RHIC and LHC on heavy ion collisions give a variety of facts in favor of production of the hot QCD matter in the quark-gluon plasma (QGP) phase. Hydrodynamic analyses of the flow effects in  $AA$  collisions at RHIC and LHC energies suggest that the QGP produced in  $AA$  collisions expands as a near-ideal liquid [1, 2]. The hydrodynamic simulations support the production time of the QGP  $\tau_0 \sim 0.5 - 1$  fm [3, 4]. However, a consistent treatment of the QGP production is presently impossible. It does not allow to impose accurate from principles initial conditions for hydrodynamic simulations of the QGP evolution in  $AA$  collisions, and requires to use phenomenological models.

At present the most popular phenomenological methods in use for determination of the initial conditions for the plasma fireball are the IP-Glasma model [5, 6] and the wounded nucleon Glauber model [7, 8]. The IP-Glasma model is based on the pQCD color-glass condensate scheme [9]. It assumes that gluon fields of the colliding nuclei can be treated perturbatively down to an infrared scale  $m_g \sim 1/R_p \sim 0.2$  GeV [5, 6] ( $R_p$  is the proton charge radius). For such a small infrared scale the gluon (and sea quark) density of the nucleon may be described as radiatively generated via the Weizsäcker-Williams fields of constituent quarks [10, 11]. In this case the perturbative dipole cross section  $\sigma_{q\bar{q}}$  of interaction of the  $q\bar{q}$  pair with a nucleon (that can be expressed via the gluon density [12]) corresponding to the double gluon exchange allows to reproduce the  $\pi p$  cross section in the tens of GeV region [13]. However, the infrared cutoff scale  $\sim 1/R_p$  is in contradiction with the fact that the inverse gluon correlation radius in the QCD vacuum  $1/R_c \sim 0.75$  GeV [14]. Because this scale, which is the natural lower limit for the virtuality scale of the perturbative gluons, is several times bigger than  $1/R_p$ . One can expect that for the  $q\bar{q}$  pair with the transverse size  $\rho \sim R_p$  the inelastic interactions are dominated by the nonperturbative process of the color flux tube rearrangement [15, 16], and the perturbative mechanism becomes dominating only at  $\rho \lesssim R_c$ . In the dipole approach to the BFKL equation [17] the data on the low- $x$  proton structure function  $F_2$  can be well described assuming that the dipole cross section contains the perturbative component with the infrared cutoff  $m_g \sim 1/R_c$  and an energy independent nonperturbative component that can be fitted to reproduce experimental pion-proton cross section [18]. It is important that in this scenario the BFKL evolution and the saturation effects in the perturbative dipole cross section with the infrared cutoff  $m_g \sim 1/R_c$  turn out to be considerably weaker than that for  $m_g \sim 1/R_p$ . The recent analysis [19] of the  $pp$  cross section in the above two component dipole scheme with  $m_g \sim 0.75$  GeV shows that the perturbative contribution turns out to be smaller than the nonperturbative one up to  $\sqrt{s} \sim 10^3$  GeV [19]. This makes questionable the accuracy of the purely perturbative schemes for calculations of the initial QGP parameters in  $AA$  collisions at RHIC and LHC energies.

The wounded nucleon Glauber model [7, 8] is a phenomenological extension of the ordinary Glauber model invented for calculations of the hadron spectra in inelastic nucleus-nucleus and hadron-nucleus collisions. In its original form [7] it was assumed that in the  $AA$  collision each nucleon undergoing inelastic soft interaction (so-called participant or wounded nucleon) produces a fixed contribution to the multiplicity rapidity density. At first this idea was purely empirical. But recently there was an attempt to give a QCD interpretation to this picture [20–22]. For particle production at midrapidity ( $\eta = 0$ ) in the center-of-mass (c.m.) frame of the colliding nuclei the contribution of each wounded nucleon equals half of the  $pp$  multiplicity rapidity density. It gives for  $AA$  collisions the multiplicity density

$\propto N_{part}$ , where  $N_{part}$  is the number of participants in both the colliding nuclei. Later, in [8] it has been proposed a two component version of the model that, in addition to the term  $\propto N_{part}$ , accounts for the hard binary collision term  $\propto N_{coll}$ . In this two component version the midrapidity multiplicity density in  $AA$  collisions takes the form

$$\frac{dN_{ch}(AA)}{d\eta} = \frac{(1-\alpha)}{2} n_{pp} N_{part} + \alpha n_{pp} N_{coll}, \quad (1)$$

where  $n_{pp} = dN_{ch}/d\eta$  is the midrapidity charged multiplicity density in  $pp$  collisions, and  $\alpha$  characterizes the fraction of hard processes to multiparticle production. In the Glauber model  $N_{part}$  and  $N_{coll}$  can be expressed through the inelastic  $pp$  cross section  $\sigma_{in}^{NN}$  and the nuclear density  $\rho_A$ . For the A+B collision of heavy nuclei at a given impact parameter  $\mathbf{b}$  in the optical approximation they read

$$N_{part}(\mathbf{b}) = \int d\rho T_A(\rho) \{1 - \exp[-T_B(\mathbf{b} - \rho)\sigma_{in}^{NN}]\} + \int d\rho T_B(\rho) \{1 - \exp[-T_A(\mathbf{b} - \rho)\sigma_{in}^{NN}]\}, \quad (2)$$

$$N_{coll}(\mathbf{b}) = \sigma_{in}^{NN} \int d\rho T_A(\rho) T_B(\mathbf{b} - \rho), \quad (3)$$

where  $T_A(\mathbf{b}) = \int dz \rho_A(\mathbf{b}, z)$  is the nuclear profile function.

It is important that the two component Glauber model allows the Monte Carlo formulation [23–25]. The Monte Carlo Glauber (MCG) model has proved to be a useful tool for analysis of the event-by-event fluctuations of observables in  $AA$  collisions. Fitting data on centrality dependence of the charged particle multiplicity density in Au+Au collisions at  $\sqrt{s} = 0.2$  TeV and in Pb+Pb collisions at  $\sqrt{s} = 2.76$  TeV gives  $\alpha \approx 0.13 - 0.15$  [26–28]. For such a value of  $\alpha$  the hard contribution to the particle production in  $AA$  collisions turns out to be rather large ( $\sim 40 - 50\%$  for central collisions). However, a considerable contribution of the binary collisions was recently questioned by the absence of the knee-like structure in the STAR data on the flow coefficient  $v_2$  in U+U collisions at  $\sqrt{s} = 193$  GeV [29] predicted in the MCG simulations of [30, 31]. In [30, 31] it was predicted that due to a prolate shape of the uranium nucleus the initial  $\epsilon_2$  should have a knee-like structure at multiplicities in the top 1% U+U collisions. The effect is related to the growth of the contribution of the binary collisions  $\propto N_{coll}$  for the tip-tip configurations of the colliding nuclei as compared to the body-body events. The knee in the elliptic flow in U+U collisions predicted in [30, 31] stimulated searches for different prescriptions for the entropy distribution in  $AA$  collisions in the Glauber picture that may be consistent with a smaller (or without) contribution of the binary collision term [32, 33].

The required contribution of the binary collision term may be smaller if the Glauber wounded nucleon model is formulated in the sub-nucleon level, when inelastic  $NN$  interactions are described as inelastic interactions of the nucleon constituents, say, quarks. The formulation of the wounded nucleon model at the quark level has been given in Refs. [34, 35]. For the wounded nucleon models with internal sub-nucleon degrees of freedom the  $dN_{ch}(AA)/d\eta$  is a nonlinear function of the number of the wounded nucleons even without the hard scattering contribution [36–40]. This is due to the growth of the fraction of the wounded constituents in each nucleon in  $AA$  collisions as compared to that in  $pp$  collisions. In this picture the two component structure (1), supported by the data, may simply be an empirical proxy for the pure quark-participant scaling of the produced entropy without (or with very small) a binary collision term at all [40]. However, the recent analysis [36] shows that in the wounded quark model the contribution to multiplicity from  $qq$  interaction required for description of data on  $AA$  collisions may differ substantially from the one that is necessary for  $pp$  collisions. Say, the data on Au+Au collisions at  $\sqrt{s} = 0.2$  TeV require the quark contribution suppressed by a factor of  $\sim 1.4$  as compared to  $pp$  interaction [36]. The results of [37] show that the situation with consistency between  $AA$  and  $pp$  collisions becomes better if the nucleon is treated as a quark-diquark system.

In previous extensions of the standard wounded nucleon Glauber model to the sub-nucleon level the sub-nucleon degrees of freedom have been assumed to be constituent quarks (or diquarks) [34–40]. However, it is well known that in the internal nucleon structure an important role is also played by the long-range meson-baryon fluctuations. Analyses of the nucleon wave function in the infinite momentum frame (IMF) show that the total weight of the meson-baryon Fock states in the nucleon may be as large as  $\sim 40\%$  [41]. These meson-baryon fluctuations are dominated by the  $\pi N$  Fock component of the physical nucleon. It is known that the effect of the pion cloud plays an important role in diffractive processes [42–44]. In the presence of the meson-baryon Fock components the diffraction excitation of the projectile proton emerges due to the well known Good-Walker mechanism [45] connected with the difference in elastic amplitudes for different Fock states. The meson-baryon Fock components are also important for inclusive processes  $pp \rightarrow n(\Delta^{++})X$  that are dominated by inelastic interaction of the pion from the projectile with the target proton [46–49]. It was understood long ago that the meson-baryon Fock components of the nucleon play an important role in the flavor dependence of nucleon parton distribution functions (PDFs) in deep inelastic scattering (DIS) [41]. It is believed that the meson-baryon Fock components are responsible for the violation of the Gottfried sum rule [41].

From the point of view of  $AA$  collisions it is important that, similarly to the wounded nucleon model with constituent quarks, in the model with the meson degrees of freedom there must be a nonlinear increase of  $dN_{ch}(AA)/d\eta$  with the number of the wounded nucleons. It is clear that this effect should emerge independently of the specific mechanism of inelastic processes.

In the present work we develop a MCG formalism which account for the meson-baryon Fock component of the physical nucleon and address its possible effect on the entropy production in  $AA$  collisions. We also study its effect in the formation of the small size plasma fireball in  $pA$  and  $pp$  collisions. Following the studies on the effect of the meson cloud on the nucleon PDFs [41] we use the IMF scheme for the meson-baryon Fock states<sup>1</sup>. We will analyze within our MCG model the available data on the charged multiplicity in Au+Au collisions at  $\sqrt{s} = 0.2$  [27] and Pb+Pb collisions at 2.76 TeV [52] and give predictions for Pb+Pb collisions at  $\sqrt{s} = 5.02$  TeV for the future LHC run 2.

The plan of the paper is as follows. In Sec. 2 we discuss the IMF model for the physical nucleon. In Sec. 2 we discuss the details of the MCG scheme. In Sec. 4 we present our numerical results. We first fix the parameters of the model from the charged multiplicity distribution in  $pp$  collisions. Then we present the results of the MCG simulations of the charged multiplicity density and azimuthal asymmetry  $\epsilon_2$  in  $AA$  collisions. We also present the results for  $pA$  and  $pp$  collisions. We give conclusions in Sec. 5. Some of our results concerning the charged multiplicity density for Au+Au and Pb+Pb collisions have been reported in an earlier short communication [53].

## II. MODEL FOR THE MESON-BARYON COMPONENT OF THE NUCLEON

Our treatment of the meson-baryon component is similar to that used in the analyses of the meson cloud effect on the nucleon PDFs (for a nice review, see [41]) based on the IMF picture of the physical nucleon wave function. At high energies this model is valid to the leading order in the nucleon energy. We write the physical nucleon IMF wave function as the Fock state composition of one- and two-body states [41, 54]

$$|N_{phys}\rangle = \sqrt{1 - n_{MB}}|N\rangle + \sum_{MB} \int dx d\mathbf{k} \Psi_{MB}(x, \mathbf{k}) |MB\rangle. \quad (4)$$

Here  $N$ ,  $B$ , and  $M$  denote the bare baryon and meson states,  $x$  is the fractional longitudinal meson momentum in the physical nucleon,  $\mathbf{k}$  is the transverse meson momentum,  $\Psi_{MB}$  is the probability amplitude for the two-body  $MB$  Fock state, and

$$n_{MB} = \sum_{MB} \int dx d\mathbf{k} |\Psi_{MB}(x, \mathbf{k})|^2 \quad (5)$$

is the total weight of the  $MB$  Fock components. The dominant two-body Fock component is the  $\pi N$  state. The IMF energy denominator of time-ordered perturbation theory for the  $MB$  component can be written as  $E_N - E_M - E_B \approx [m_N^2 - M_{MB}^2(x, \mathbf{k}^2)]/2E_N$ , where

$$M_{MB}^2(x, \mathbf{k}^2) = \frac{m_M^2 + \mathbf{k}^2}{x} + \frac{m_B^2 + \mathbf{k}^2}{1 - x} \quad (6)$$

is the squared invariant mass of the two-body  $MB$  system.

The IMF wave function of the  $MB$  Fock component (for point-like particles) may be written as

$$\Psi_{MB}(x, \mathbf{k}) = \frac{\langle MB|V|N\rangle}{4\pi^{3/2} \sqrt{x(1-x)} [m_N^2 - M_{MB}^2(x, \mathbf{k})]}. \quad (7)$$

Eq. (7) corresponds to the wave function normalization of Eq. (5). Here  $\langle MB|V|N\rangle$  is the vertex factor in the IMF-limit, which depends on the form of the Lagrangian. For the dominating  $\pi N$  state the vertex reads  $\langle \pi N'|V|N\rangle = g_{\pi NN} \bar{u}_{N'} \gamma_5 u_N$  (the helicity dependent vertex functions for different  $MB$  states can be found in [41]). The internal structure of the hadrons is accounted for by multiplying the vertex factor for point-like particles by a phenomenological

---

<sup>1</sup> Note that our calculations, from the point of view of the inelastic cross sections correspond the account for the effect of the inelastic Gribov rescatterings [50]. But one should bear in mind that from the point of view of charged multiplicity density the wounded nucleon scheme is not equivalent to calculations in the Glauber model with the AGK rules that without Pomeron interactions give for A+B nuclear collisions  $\frac{dN_{ch}(AA)}{d\eta} = ABn_{pp}$  in the central rapidity region [51].

formfactor,  $F$ . To insure the charge and momentum conservation for the IMF wave functions the formfactor should depend on  $x$  and  $\mathbf{k}$  only via the invariant mass  $M_{MB}(x, \mathbf{k})$  [41, 54–56]. The information on the phenomenological formfactor  $F$  for the dominating  $\pi N$  component may be extracted from the data on the neutron spectrum in the process  $pp \rightarrow nX$ . The analysis [57] of the experimental neutron spectrum within the IMF formalism with the dipole formfactor [56]

$$F = \left( \frac{\Lambda^2 + m_N^2}{\Lambda^2 + M_{\pi N}^2(x, \mathbf{k})} \right)^2 \quad (8)$$

gives  $\Lambda \approx 1.3$  GeV. It is also supported by the data on the nucleon PDFs, because at the same time it allows to describe the violation of the Gottfried sum rule [41]. In Fig. 1 we show the  $x$ -distribution for the  $\pi N$  state for this value of the parameter  $\Lambda$ . One can see that the spectrum is peaked at  $x \sim 0.3$ . For the  $\rho$ -meson the spectrum is peaked at somewhat larger  $x$  ( $x \sim 0.5$  [41]). The transverse distribution for the  $\pi N$  state at  $x = 0.3$  is shown in

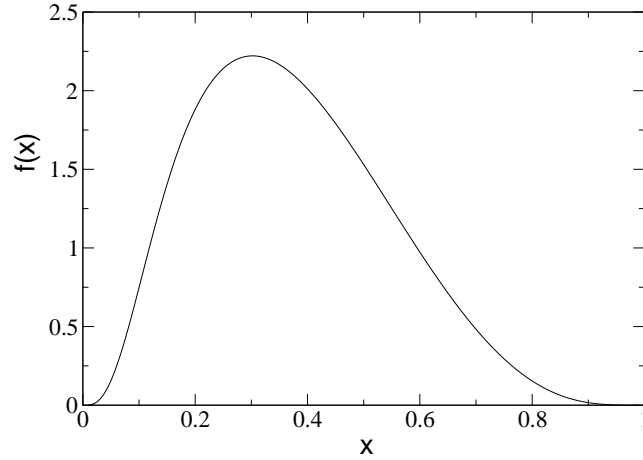


FIG. 1: Normalized to unity longitudinal  $x$ -distribution for the  $\pi N$  Fock component obtained for the dipole formfactor (8) with  $\Lambda = 1.3$  GeV.

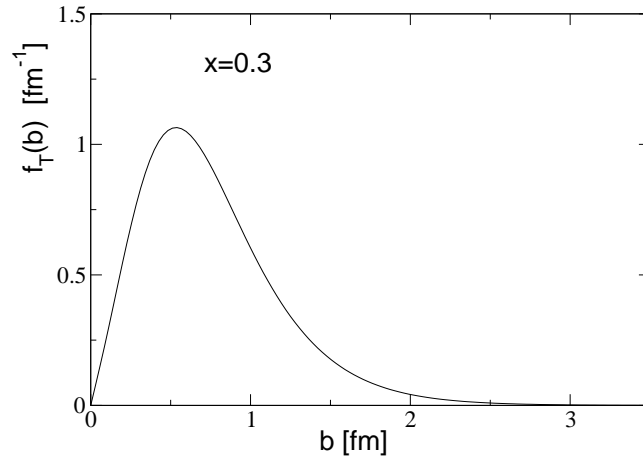


FIG. 2: Transverse distribution versus  $b$  for the  $\pi N$  state at  $x = 0.3$  for the dipole formfactor (8) with  $\Lambda = 1.3$  GeV with the normalization  $\int db f_T(b) = 1$ .

Fig. 2. It gives for the root mean square transverse radius of the  $\pi N$  component  $\langle \rho_{\pi N}^2 \rangle^{1/2} \approx 0.87$  fm.

The IMF scheme allows one to avoid the difficulties with the momentum and charge conservation present in the earlier analyses of the effects of the meson cloud in DIS based on the covariant formulation [58, 59]. For the formfactor  $F$  depending on the  $M_{MB}(x, \mathbf{k})$  the meson and baryon  $x$ -distributions of the physical nucleon satisfy the relation

$$f_{M/N}(x) = f_{B/N}(1 - x), \quad (9)$$

where

$$f_{M/N}(x) = \int d\mathbf{k} |\Psi(x, \mathbf{k})|^2, \quad (10)$$

and

$$f_{B/N}(x) = \int d\mathbf{k} |\Psi(1-x, \mathbf{k})|^2. \quad (11)$$

The symmetry relation (9) between the  $N \rightarrow M$  and  $N \rightarrow B$  splitting functions is not satisfied in the covariant description of the meson cloud with phenomenological formfactors depending on the invariant variable  $t$  [41, 55].

In DIS the meson and baryon in the two-body Fock states act as an independent sources of the parton distributions [41, 56]. The results of the previous analyses of the meson cloud effects in DIS show that to a good accuracy in the Fock state decomposition (2) it is enough to include  $\pi N$ ,  $\pi\Delta$ ,  $\rho N$  and  $\rho\Delta$  two-body systems. The total weight of these four two-body states in the physical nucleon is about 40% [41]. The representation (4) neglects the higher order terms from many-body systems. A qualitative analysis [55] show that the effect of the higher order Fock states should be relatively small for realistic formfactors. We assume that the soft inelastic  $NN$  interaction may be described as independent inelastic interactions of the bare meson and baryon constituents of the colliding nucleons. The specific mechanism of the inelastic interactions of the bare constituents is not crucial at this point<sup>2</sup>. Because the quark contents of the bare  $\Delta$  and  $\rho$ -meson are the same as for the bare  $N$  and  $\pi$  states, we make a reasonable assumption that from the point of view of inelastic interactions the bare  $\Delta$  is equivalent to the bare  $N$  state and the  $\rho$ -meson is equivalent the pion. Then, in the wounded nucleon picture each physical nucleon interacts with the probability  $1 - n_{MB}$  as the bare  $N$  and with the probability  $n_{MB}$  as the two-body  $\pi N$  system. Since the dominating  $\pi N$  state is peaked at  $x \approx 0.3$  we, for the sake of simplicity, take for the fractional meson momentum in the effective  $MB$  component  $x = 0.3$ . For the transverse spacial distribution of the  $MB$  state we use the distribution of the dominant  $\pi N$  component at  $x = 0.3$  shown in Fig. 2. We renormalized it to match the total weight of the  $\pi N$ ,  $\pi\Delta$ ,  $\rho N$  and  $\rho\Delta$  components  $n_{MB} = 0.4$  [41]. Note that the results of the MCG simulation are not very sensitive to the value of  $\Lambda$ . This is because there is no shadowing effects for inelastic interactions of the baryon and meson constituents.

### III. FORMULATION OF THE MCG SCHEME

For the two component model of the nucleon (4) inelastic interaction of the physical nucleons from the colliding objects occurs as  $N + N$ ,  $N + MB$ ,  $MB + N$  and  $MB + MB$  collisions. We assume that the inelastic cross sections for the bare states obey the constituent quark counting rule  $4\sigma_{in}^{NN} = 6\sigma_{in}^{MB} = 9\sigma_{in}^{MM}$ . For the impact parameter profile of the probability of  $ab$  inelastic interaction we use a Gaussian form

$$P_{ab}(\rho) = \exp(-\pi\rho^2/\sigma_{in}^{ab}). \quad (12)$$

We adjusted the value of the parameter  $\sigma_{in}^{NN}$  to reproduce the experimental inelastic  $pp$  cross section  $\sigma_{in}^{pp}$  (see below).

We consider the charged multiplicity density  $dN_{ch}/d\eta$  at the central pseudorapidity  $\eta = 0$  (sometimes, for clarity, we will use for  $dN_{ch}/d\eta$  a simple notation  $N_{ch}$  assuming that the charged multiplicity is defined in the unit pseudorapidity window  $|\eta| < 0.5$ ). For calculation of the contribution to the multiplicity density from the  $MB$  component we need to know the  $dN_{ch}/d\eta$  for pion-nucleon and pion-pion collisions. The direct data for pion-proton and pion-pion collisions for RHIC-LHC energies are absent. We use the information from the quark-gluon string model [60, 61]. Calculations within this model show that the charged particle multiplicity density in the central rapidity region for  $\pi p$  and  $\pi\pi$  collisions is somewhat bigger than that in  $pp$  collisions. Our calculations show that to good accuracy this small excess compensates a possible reduction of the multiplicity density in  $\pi p$  and  $\pi\pi$  interactions due to somewhat smaller c.m. energy in our model. For this reason we, for the sake of simplicity, assume that all the wounded bare particles produce the same amount of entropy per unit rapidity in the c.m. frame of colliding objects. We ignore the effect of a small

---

<sup>2</sup> We restrict ourselves to the leading order contribution from the meson and baryon degrees of freedom of the physical nucleon in the IMF. Of course, each meson/baryon constituent develops its own IMF wave function at the quark-gluon level, that is important from the point of view the inelastic interactions of the meson/baryon constituents. As it occurs, say, in the IT-Glasma model [5, 6]. In principle, higher order meson/baryon Fock states in the IMF wave function also can contribute to the inelastic interactions of the bare meson/baryon states. However, in the wounded nucleon Glauber model this complicated dynamics is replaced by the simple phenomenological ansatz on the entropy production from inelastic interactions of the bare meson/baryon constituents.

rapidity shift ( $\sim 0.5$ ) of the c.m. frame for pairs with different energies (as it occurs for  $\pi N$  interactions) on the entropy rapidity density, because the charged multiplicity density is almost flat at midrapidity.

The total entropy rapidity density of the fireball for the A+B collision is the sum of the contributions from the sources corresponding to the wounded constituents and to the binary collisions of the constituents

$$\frac{dS}{dy} = \sum_{i=1}^{N_w} \frac{dS_w^i}{dy} + \sum_{i=1}^{N_{bin}} \frac{dS_{bin}^i}{dy}, \quad (13)$$

where

$$\frac{dS_w^i}{dy} = \frac{(1-\alpha)}{2} S \quad (14)$$

is the contribution of individual source from the wounded constituents in the systems A and B, and

$$\frac{dS_{bin}^i}{dy} = S \quad (15)$$

is the contribution of individual binary collision. In the MCG simulations we assume that for each pair of wounded particles the probability of a hard binary collision is  $\alpha$ . As usually done in the MCG schemes, to model the fluctuations of the multiplicity density in  $pp$  collisions, we treat the quantity  $S$  in (14), (15), as a random variable. We assume an isentropic evolution of the fireball. For the isentropic expansion the initial entropy rapidity density is proportional to the final charged multiplicity pseudorapidity density

$$dS/dy = C dN_{ch}/d\eta, \quad (16)$$

where  $C \approx 7.67$  [62]. In this approximation we can work directly with the pseudorapidity charged particle density  $dN_{ch}/d\eta$ . So we will treat each fluctuating entropy source as a source producing a fluctuating amount  $n = S/C$  of charged particles in the unit pseudorapidity interval  $|\eta| < 0.5$ . We describe the fluctuations of  $n$  for each source by the Gamma distribution

$$\Gamma(n, \langle n \rangle) = \left( \frac{n}{\langle n \rangle} \right)^{\kappa-1} \frac{\kappa^\kappa \exp[-n\kappa/\langle n \rangle]}{\langle n \rangle \Gamma(\kappa)}, \quad (17)$$

which is widely used in the MCG simulations. We adjusted the parameters  $\langle n \rangle$  and  $\kappa$  to the experimental  $pp$  data on the mean charged multiplicity and its variance in the unit pseudorapidity window  $|\eta| < 0.5$  (see below). Our calculations show that for  $AA$  collisions the results for the Gamma distributions are very similar to that for the negative binominal distribution.

In comparison with experimental data we, as usual, define the centrality  $c$  in  $AA$  collisions through the theoretical charged multiplicity distribution  $P$  [63]

$$c(N_{ch}) = \sum_{N=N_{ch}}^{\infty} P(N). \quad (18)$$

Here  $N_{ch}$  is the theoretical charged multiplicity for  $|\eta| < 0.5$ , i.e.  $dN_{ch}/d\eta$  in our MCG simulations. For calculation of the centrality dependence of the charged particle multiplicity the distribution of the entropy rapidity density in the transverse coordinates is not important. However, the spacial distribution of the deposited entropy is important for the geometric quantities, such as the initial anisotropy coefficients  $\epsilon_n$  of the fireball. In terms of the spacial entropy distribution (we denote it by  $\rho_s = dS/dy d\boldsymbol{\rho}$ ) the coefficients  $\epsilon_n$  read [64, 65]

$$\epsilon_n = \frac{|\int d\boldsymbol{\rho} \rho^n e^{in\phi} \rho_s(\boldsymbol{\rho})|}{\int d\boldsymbol{\rho} \rho^n \rho_s(\boldsymbol{\rho})} \quad (19)$$

(here it is assumed that the transverse vectors  $\boldsymbol{\rho}$  are calculated in the transverse c.m. frame, i.e.,  $\int d\boldsymbol{\rho} \boldsymbol{\rho} \rho_s(\boldsymbol{\rho}) = 0$ ). For the point-like sources we have

$$\rho_s(\boldsymbol{\rho}) = \sum_{i=1}^{N_w} \delta(\boldsymbol{\rho} - \boldsymbol{\rho}_i) \frac{dS_w^i}{dy} + \sum_{i=1}^{N_{bin}} \delta(\boldsymbol{\rho} - \boldsymbol{\rho}_i) \frac{dS_{bin}^i}{dy}. \quad (20)$$

We use the popular prescription that for the wounded constituents the centers of the sources are located at the positions of the wounded particles, and that for each binary collision the source is located in the middle between colliding particles. Of course, physically, the approximation of the point-like sources is clearly unreasonable. We account for qualitatively the finite size of the sources by replacing the  $\delta$  functions in (20) by a Gaussian distribution

$$\exp(-\rho^2/\sigma^2)/\pi\sigma^2. \quad (21)$$

We perform calculations for  $\sigma = 0.7$  and  $0.4$  fm. The results for the anisotropy coefficients in  $AA$  collisions become sensitive to the width of smearing of the sources only for very peripheral collisions, but for the small size fireballs in  $pA$  and  $pp$  collisions the value of  $\sigma$  is very crucial (see below).

We perform calculations for the Woods-Saxon nuclear distribution. We account for the deformation for the nuclei  $^{197}\text{Au}$  and  $^{238}\text{U}$ . For these nuclei we use the  $\theta$ -dependent Woods-Saxon nuclear density

$$\rho_A(r, \theta) = \frac{\rho_0}{1 + \exp[(r - R_A(\theta)/a)]}, \quad (22)$$

$$R_A(\theta) = R[1 + \beta_2 Y_{20}(\theta) + \beta_4 Y_{40}(\theta)] \quad (23)$$

with  $Y_{20}$  and  $Y_{40}$  the spherical harmonics. Following [25] we take  $R = 6.37(6.8)$  fm,  $\beta_2 = -0.13(0.28)$ , and  $\beta_4 = -0.03(0.093)$  for Au(U) nuclei, and  $a = 0.54$  fm. For the  $^{207}\text{Pb}$  nucleus we use the ordinary spherically symmetrical Woods-Saxon formula with a  $\theta$ -independent ( $\beta_{02} = \beta_{04} = 0$ ) radius  $R_A = (1.12A^{1/3} - 0.86/A^{1/3}) = 6.49$  fm, and  $a = 0.54$  fm [25].

## IV. NUMERICAL RESULTS

### A. Parameters of the model for $pp$ collisions

In numerical calculations for  $pp$  collisions we take  $n_{pp} = 2.65$  at  $\sqrt{s} = 0.2$  TeV obtained by the UA1 collaboration [66] for non-single-diffractive (NSD) events. For NSD  $pp$  events at  $\sqrt{s} = 2.76$  TeV we use the ALICE result  $n_{pp} \approx 4.63$

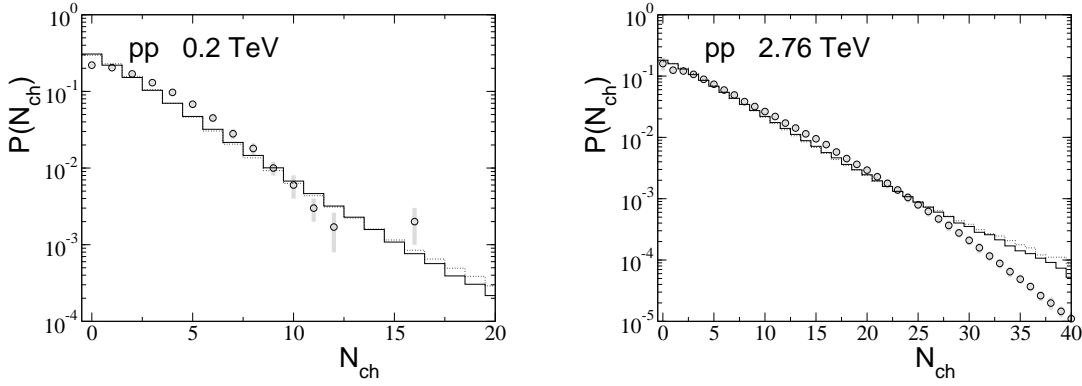


FIG. 3: Charged multiplicity distribution in  $pp$  collisions for the pseudorapidity window  $|\eta| < 0.5$ . Left: MCG simulation for  $\sqrt{s} = 0.2$  TeV for the scenario with the meson cloud for  $\alpha = 0.06$  (solid) and without the meson cloud for  $\alpha = 0.135$  (dotted), the data are from UA5 [69]. Right: MCG simulation for  $\sqrt{s} = 2.76$  TeV for the scenario with the meson cloud for  $\alpha = 0.09$  (solid) and without the meson cloud for  $\alpha = 0.14$  (dotted), the data are from ALICE [67].

[67]. In the MCG simulations for  $\sigma_{in}^{pp}$  we also use the inelastic  $pp$  cross section corresponding to the NSD event class. The exclusion of the diffractive contribution is reasonable because the diffractive events do not contribute to the midrapidity multiplicity density considered in the present work. We use for the NSD  $pp$  inelastic cross section at  $\sqrt{s} = 0.2$  TeV the value 35 mb measured by the UA1 collaboration [66]. For  $\sqrt{s} = 2.76$  TeV we use the value 50.24 mb obtained by the ALICE collaboration [68]. With the above values of the NSD  $\sigma_{in}^{pp}$  we fitted  $\sigma_{in}^{NN}$  for the bare nucleons necessary for the MCG simulations in the version with the  $MB$  Fock component. For this version we obtained

$$\sigma_{in}^{NN}[\sqrt{s} = 0.2, 2.76 \text{ TeV}] \approx [26.15, 38.4] \text{ mb}. \quad (24)$$

For the version without the meson cloud the parameter  $\sigma_{in}^{NN}$  is equal simply to the experimental NSD  $pp$  cross section. We fitted the parameters  $\langle n \rangle$  and  $\kappa$  of the Gamma distribution (17) to reproduce the experimental mean  $N_{ch}$  in  $pp$  collisions and to satisfy the relation  $N_{ch}/D = 1$  ( $D^2$  is a variance of  $N_{ch}$ ) in the pseudorapidity window  $|\eta| < 0.5$ , which is well satisfied for the experimental multiplicity distribution both at  $\sqrt{s} = 0.2$  TeV [66] and at  $\sqrt{s} = 2.76$  TeV [67]. For the scenario without the meson cloud the parameter  $\langle n \rangle$  should be equal to the experimental  $dN_{ch}/d\eta$  for any fraction of the binary collisions  $\alpha$ . But the value of the parameter  $\kappa$  depends on  $\alpha$ . At  $\alpha = 0$  the relation  $N_{ch}/D = 1$  gives  $\kappa = 0.5$ . For  $\alpha > 0$  the value of  $\kappa$  grows weakly with  $\alpha$ . But the deviation from 0.5 is relatively small. For the scenario with the  $MB$  component  $\kappa$  is also close to 0.5, and the required value of  $\langle n \rangle$  is smaller than the experimental mean  $N_{ch}$ .

To determine the values of the parameter  $\alpha$  we used a two step procedure. First, we fitted the parameters  $\langle n \rangle$  and  $\kappa$  to the  $pp$  data on  $N_{ch}$  imposing the condition  $N_{ch}/D = 1$  for a broad set of  $\alpha$  from 0 to 0.2. In the second step, we used the set of  $\langle n \rangle$  and  $\kappa$  to fit the parameter  $\alpha$  to best reproduce the data on the centrality dependence of the midrapidity  $dN_{ch}/d\eta$  in Au+Au collisions at  $\sqrt{s} = 0.2$  TeV from STAR [27] and in Pb+Pb collisions at  $\sqrt{s} = 2.76$  TeV from ALICE [52]. For Au+Au collisions at  $\sqrt{s} = 0.2$  TeV this procedure gives  $\alpha \approx 0.06$  and  $\alpha \approx 0.135$  for the scenarios with and without the meson cloud, respectively. From the ALICE data on Pb+Pb collisions at  $\sqrt{s} = 2.76$  TeV [52] we obtained  $\alpha \approx 0.09$  and  $\alpha \approx 0.14$  for the scenarios with and without the meson cloud, respectively. The parameters of the Gamma distribution (17) obtained from the fit with the meson cloud to the  $pp$  data for the above optimal values of  $\alpha$  read

$$\langle n \rangle[\sqrt{s} = 0.2, 2.76 \text{ TeV}] \approx [2.39, 4.13], \quad (25)$$

$$\kappa[\sqrt{s} = 0.2, 2.76 \text{ TeV}] \approx [0.506, 0.52]. \quad (26)$$

For the scenario without the meson cloud for the optimal values of  $\alpha$  we obtained

$$\kappa[\sqrt{s} = 0.2, 2.76 \text{ TeV}] \approx [0.57, 0.57], \quad (27)$$

(as we said  $\langle n \rangle$  is equal to the experimental  $n_{pp}$ ). As one could expect a priori, accounting for the meson cloud leads to a reduction of the required fraction of the binary collisions. The effect becomes somewhat smaller at the LHC energy. This is natural because the interaction radius becomes bigger at the LHC energies. It results in a lower sensitivity to the internal nucleon structure.

In Fig. 3 we compare the multiplicity distribution of charged hadrons for the versions with and without the meson cloud for  $|\eta| < 0.5$  for  $pp$  collisions at  $\sqrt{s} = 0.2$  TeV and  $\sqrt{s} = 2.76$  TeV with the experimental data from UA5 [69] and ALICE [67]. One sees that for both of the versions the agreement with the data are reasonable in the region  $N_{ch} \lesssim 5\langle N_{ch} \rangle$ . Note however, that the multiplicity distributions in  $AA$  collisions is not very sensitive to the specific form of the multiplicity distribution in  $pp$  collisions except for the region of very peripheral collisions when the number of the wounded nucleons becomes small. Anyway, the tail region of the charged multiplicity distribution with  $N_{ch} \gg \langle N_{ch} \rangle$  practically cannot affect the theoretical predictions for  $AA$  collisions.

## B. A+A collisions: charged multiplicity density

In Figs. 4, 5 we compare our results for centrality dependence of the charged multiplicity density  $dN_{ch}/d\eta$  at  $\eta = 0$  for the fitted values of  $\alpha$  with the STAR data on Au+Au collisions at  $\sqrt{s} = 0.2$  TeV [27] and the ALICE data on Pb+Pb collisions at  $\sqrt{s} = 2.76$  TeV [52]. The theoretical histograms have been obtained by Monte Carlo generation of samples with  $\sim 2 \times 10^6$  events. As was noted earlier, our parameters of the Gamma distribution (17) and the definition of centrality for  $AA$  collisions (18) correspond to the unit pseudorapidity window  $|\eta| < 0.5$ . The centrality categorization in the STAR data [27] and the ALICE data [52] is also performed via the charged multiplicity at  $|\eta| < 0.5$ . However, in principle, for collisions of heavy nuclei it is not very crucial because the effect of the multiplicity fluctuations at a given impact parameter (except for very peripheral collisions) on the centrality categorization of a given event is small [63]. To illustrate better the magnitude of the effect of the meson cloud we show in Figs. 4a and 5a the results for the scenario without the meson cloud, but obtained with the optimal  $\alpha$  for the scenario with the meson cloud. Comparison of the two histograms show that at small centrality the meson cloud increases the multiplicity by  $\sim 16 - 18\%$ . Since our calculations do not assume a certain mechanism of the entropy production in collisions of the bare baryon and meson states, one can expect that the  $MB$  Fock components in the nucleon wave function should increase the multiplicity in  $AA$  collisions in any scheme.

In the future LHC run 2 Pb+Pb collisions will be studied at  $\sqrt{s} = 5.02$  TeV. To give the theoretical prediction for Pb+Pb collisions at this energy we have used the same values of the parameter  $\alpha$  as for  $\sqrt{s} = 2.76$  TeV. Since the



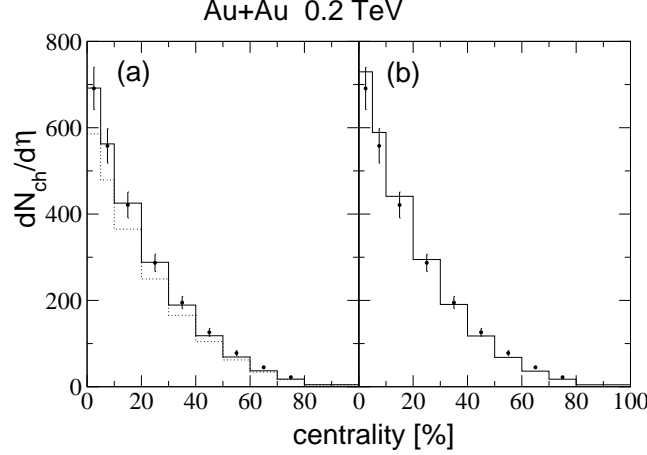


FIG. 4: Centrality dependence of  $dN_{ch}/d\eta$  at  $\eta = 0$  for Au+Au collisions at  $\sqrt{s} = 0.2$  TeV. Left: MCG simulation for the scenarios with (solid) and without (dotted) the meson cloud for  $\alpha = 0.06$ . Right: MCG simulation for the scenario without the meson cloud for  $\alpha = 0.135$ . Data are from STAR [27].

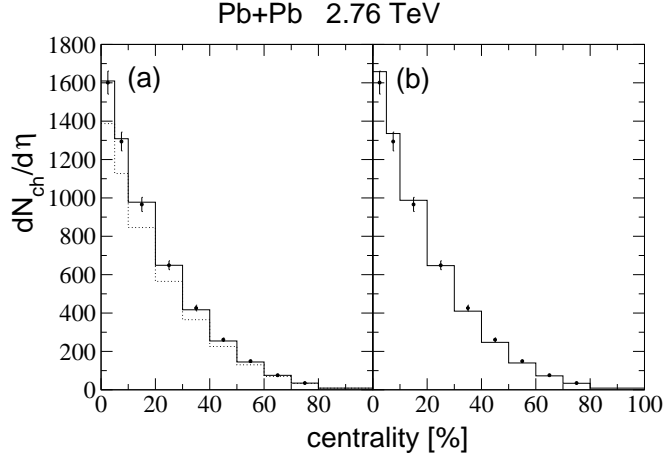


FIG. 5: Centrality dependence of  $dN_{ch}/d\eta$  for Pb+Pb collisions at  $\sqrt{s} = 2.76$  TeV. Left: MCG simulation for the scenarios with (solid) and without (dotted) the meson cloud for  $\alpha = 0.09$ . Right: MCG simulation for the scenario without the meson cloud for  $\alpha = 0.14$ . Data are from ALICE [52].

variation of  $\alpha$  from  $\sqrt{s} = 0.2$  TeV to  $\sqrt{s} = 2.76$  TeV is not strong, one can expect that its variation from  $\sqrt{s} = 2.76$  TeV to  $\sqrt{s} = 5.02$  TeV should not be significant. The direct  $pp$  data on  $dN_{ch}/d\eta$  at  $\sqrt{s} = 5.02$  TeV are absent. We obtained it with the help of the power law interpolation  $dN_{ch}/d\eta \propto s^\delta$  between the ALICE data [67] at  $\sqrt{s} = 2.76$  TeV ( $dN_{ch}/d\eta \approx 4.63$ ) and at  $\sqrt{s} = 7$  TeV ( $dN_{ch}/d\eta = 5.74 \pm 0.15$ ). It gives  $dN_{ch}/d\eta \approx 5.35$  at  $\sqrt{s} = 5.02$  TeV. We use for the NSD  $pp$  inelastic cross section at  $\sqrt{s} = 5.02$  TeV the value 55.44 mb obtained by interpolating between the ALICE data [68] at  $\sqrt{s} = 2.76$  and 7 TeV. Making use of the above NSD  $\sigma_{in}^{pp}$  we fitted the parameter  $\sigma_{in}^{NN}$  for the scenario with the meson cloud for  $\alpha = 0.09$ . We obtained  $\sigma_{in}^{NN}(\sqrt{s} = 5.02 \text{ TeV}) \approx 42.49$  mb (as in the analysis of for  $\sqrt{s} = 2.76$  TeV for the scenario without the meson cloud  $\sigma_{in}^{NN}$  is equal to the NSD  $pp$  cross section). As above, the parameters  $\langle n \rangle$  and  $\kappa$  of the Gamma distribution (17) have been fitted to reproduce the experimental  $n_{pp}$  and to satisfy the relation  $n_{pp}/D = 1$ . Without the meson cloud  $\langle n \rangle$  is simply equal to the interpolation of the experimental  $dN_{ch}/d\eta$  between  $\sqrt{s} = 2.76$  and 7 TeV, and fit of  $\kappa$  for  $\alpha = 0.14$  gives  $\kappa = 0.564$ . For the scenario with the meson cloud we obtained  $\langle n \rangle \approx 4.72$ , and  $\kappa \approx 0.52$ . In Fig. 6 we compare our results for centrality dependence of the charged multiplicity in Pb+Pb at  $\sqrt{s} = 5.02$  TeV and at  $\sqrt{s} = 2.76$  TeV. From Fig. 6 one sees that as compared to  $\sqrt{s} = 2.76$  the growth of  $dN_{ch}/d\eta$  in the central Pb+Pb collisions for  $\sqrt{s} = 5.02$  TeV is about 20%. It corresponds to increase of the fireball initial temperature by  $\sim 6\%$ .

As was noted, in the scheme with the meson cloud the contribution of soft processes to the multiplicity density is not proportional to the number of wounded nucleons, because the probability of inelastic interactions of the meson states depends on centrality. To illustrate the variation with centrality of the contribution of each wounded nucleon

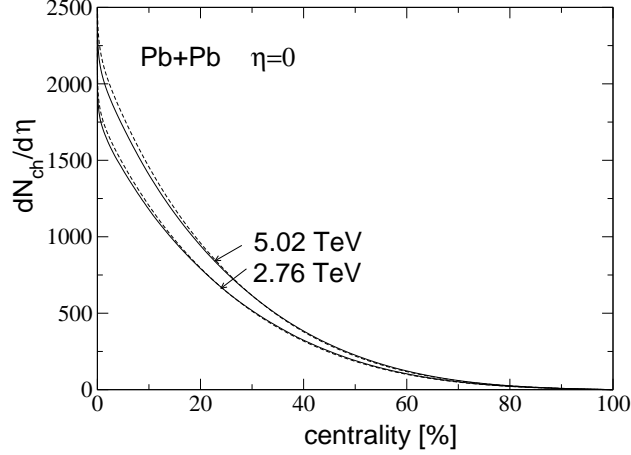


FIG. 6: Comparison of the centrality dependence of  $dN_{ch}/d\eta$  at  $\eta = 0$  for Pb+Pb collisions at  $\sqrt{s} = 2.76$  and 5.02 TeV obtained from the MCG simulation for the scenarios with (solid) the meson cloud for  $\alpha = 0.09$  and without (dashed) the meson cloud for  $\alpha = 0.14$ .

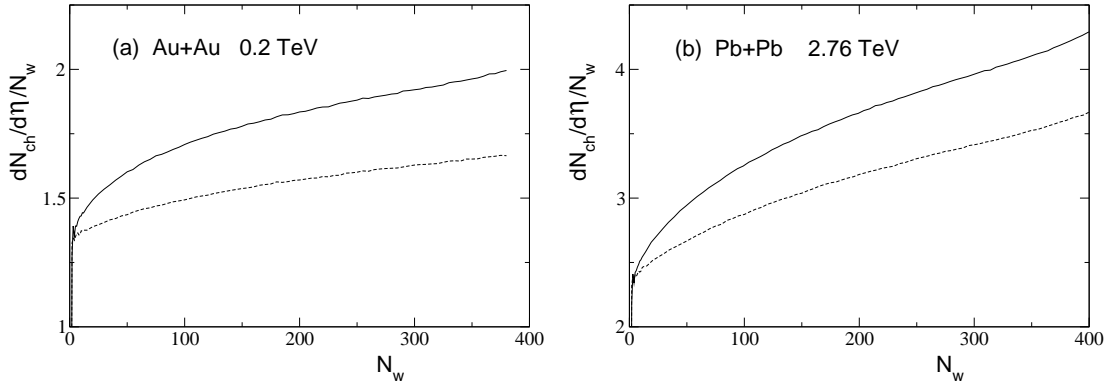


FIG. 7: Ratio  $dN_{ch}/d\eta/N_w$  versus the number of the wounded nucleons  $N_w$ . Left: MCG simulation for Au+Au collisions at  $\sqrt{s} = 0.2$  TeV for the scenarios with (solid) and without (dashed) the meson cloud for  $\alpha = 0.06$ . Right: MCG simulation for Pb+Pb collisions at  $\sqrt{s} = 2.76$  TeV for the scenarios with (solid) and without (dashed) the meson cloud for  $\alpha = 0.09$ .

due to the *MB* component in Fig. 7 we plot the ratio  $dN_{ch}/d\eta/N_w$  as a function of  $N_w$  obtained with and without the *MB* component for the same  $\alpha$  ( $\alpha = 0.06$  for Au+Au collisions at  $\sqrt{s} = 0.2$  TeV and  $\alpha = 0.09$  for Pb+Pb collisions at  $\sqrt{s} = 2.76$  TeV). One sees that from peripheral to central collisions this ratio rises by  $\sim 20\%$  and  $\sim 15\%$  for RHIC and LHC conditions, respectively.

### C. A+A collisions: azimuthal eccentricity of the fireball

We have also studied the effect of the *MB* component on the root mean square (rms) anisotropy coefficient  $\epsilon_2$  (which is often noted as  $\epsilon_2\{2\}$ ). In Fig. 8 we present the results for the rms  $\epsilon_2$  versus centrality for Au+Au at  $\sqrt{s} = 0.2$  TeV and Pb+Pb at  $\sqrt{s} = 2.76$  TeV for the two models. We present the results for two values of the Gaussian width of the sources  $\sigma = 0.7$  and 0.4 fm. One sees that for small centrality the results with and without the meson cloud are close to each other. For noncentral collisions with centrality  $\lesssim 80\%$  the version with the meson cloud gives a little smaller  $\epsilon_2$ . But for very peripheral collisions with centrality  $\gtrsim 80\%$  the anisotropy for the model with the meson cloud becomes bigger than that without the meson cloud. The dependence of the asymmetry on  $\sigma$  is rather weak, except for the region of large centrality ( $\gtrsim 60 - 70\%$ ), where the typical number of sources is small and the results become sensitive to the shape of the entropy distribution in individual *NN* collisions. Of course, in this region the results are very model dependent and not robust. Thus we found that the effect of the meson cloud on the eccentricity  $\epsilon_2$  in *AA* collisions is relatively small.

Recently there has been considerable interest in the centrality/multiplicity dependence of the eccentricity  $\epsilon_2$  for

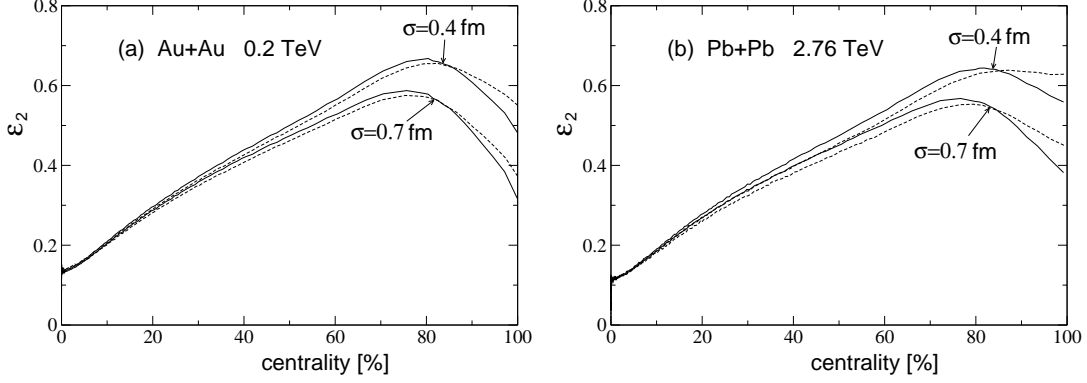


FIG. 8: Centrality dependence of the rms  $\epsilon_2$  for the Gaussian source distribution (21) for  $\sigma = 0.7$  and  $0.4$  fm. Left: MCG simulation for Au+Au collisions at  $\sqrt{s} = 0.2$  TeV for the scenarios with (solid) the meson cloud for  $\alpha = 0.06$  and without (dashed) the meson cloud for  $\alpha = 0.135$ . Right: MCG simulation for Pb+Pb collisions at  $\sqrt{s} = 2.76$  TeV for the scenarios with (solid) the meson cloud for  $\alpha = 0.09$  and without (dashed) the meson cloud for  $\alpha = 0.14$ .

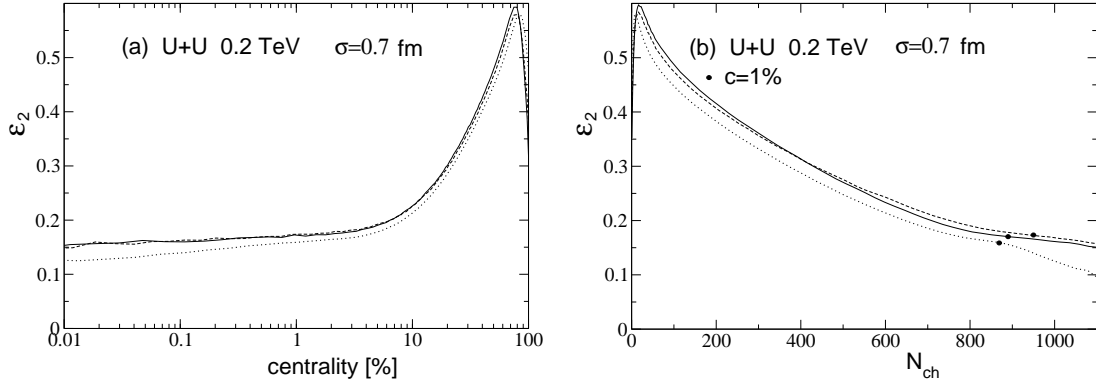


FIG. 9: Centrality (left) and  $N_{ch}$  (right) dependence of the rms  $\epsilon_2$  for U+U collisions at  $\sqrt{s} = 0.2$  TeV obtained for the Gaussian source distribution (21) for  $\sigma = 0.7$  fm. Solid: MCG simulation for the scenario with the meson cloud for  $\alpha = 0.06$ . Dashed: MCG simulation for the scenario without the meson cloud for  $\alpha = 0.135$ . Dotted: MCG simulation for the scenario without the meson cloud for  $\alpha = 0.135$  without fluctuations of the charged multiplicity in  $NN$  collisions for  $n_{pp} = 2.65$ . In the right panel the dots mark the points with  $c = 1\%$ .

U+U collisions [30–33] due to expected sensitivity of the multiplicity to orientation of the colliding nuclei connected with the prolate shape of the  $^{238}\text{U}$ -nucleus. In [30, 31] it was predicted that in U+U collisions the initial asymmetry  $\epsilon_2$  should have a knee structure at multiplicities in the top 1% central U+U collisions (the knee-like structure has also been found in the recent MCG simulation of [33]). It may be interpreted as due to the growth of the relative contribution of the binary collisions for the tip-tip configurations of the colliding nuclei for a nonzero fraction  $\alpha$  of the  $\propto N_{coll}$  term in the MCG scheme. However the elliptic flow  $v_2$  measured by STAR [29] in U+U collisions at  $\sqrt{s} = 193$  GeV shows no indication of such a knee structure. This challenged the two component Glauber model with a significant contribution of the binary collisions, and stimulated searches for alternative ansatze for the entropy generation in the Glauber picture [32, 33]. But it worth noting that the theoretical situation with the knee in the  $\epsilon_2$  for the standard two component MCG model is still somewhat controversial. Indeed, the analysis [30] has been performed neglecting the fluctuations of the multiplicity in  $NN$  collisions. But in [31, 33] the fluctuations of the charged multiplicity in  $NN$  collisions have been taken into account. However, later in [70] it was demonstrated that the knee structure vanishes when the fluctuations are taken into account, that is in contradiction with the analyses [31, 33]. On the other hand, more recent analysis [71] indicates on appearance of a weak knee-like feature even when the multiplicity fluctuations in  $NN$  collisions are taken into account. In Fig. 9a we show our results for  $\epsilon_2$  versus centrality in U+U collisions at  $\sqrt{s} = 0.2$  TeV for the source width  $\sigma = 0.7$  fm. To stretch the region of small centralities a logarithmic scale is used. One can see that the predictions for the rms  $\epsilon_2$  in the centrality region  $0.01 \lesssim c \lesssim 1\%$  for the versions with and without the  $MB$  component are very similar. In this region  $\epsilon_2$  decreases very smoothly with  $c$ , and does not have a knee-like structure. In Fig. 9a we also plot the prediction of the MCG simulation without the meson cloud obtained without fluctuations of the multiplicity in  $pp$  collisions. The ellipticity in this case

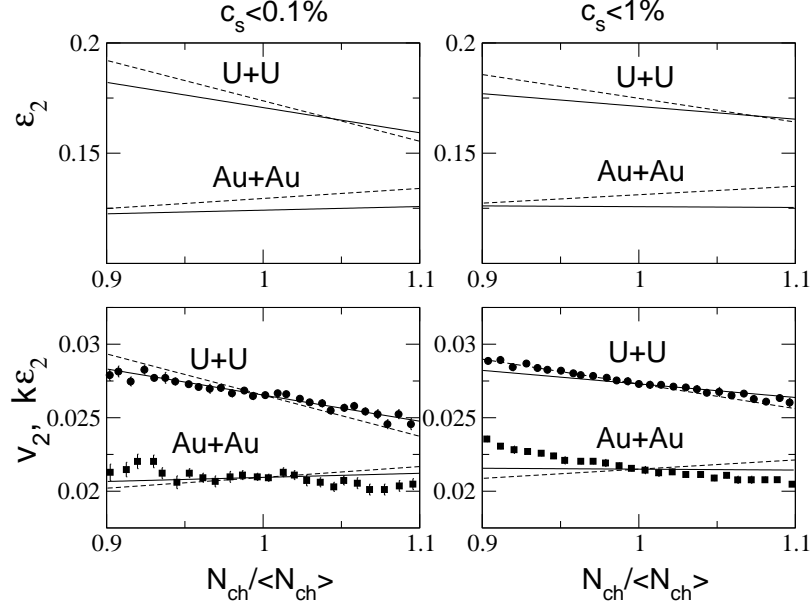


FIG. 10: rms ellipticity  $\epsilon_2$  (upper panels) and  $v_2$  (lower panels) versus  $N_{ch}/\langle N_{ch} \rangle$  in Au+Au and U+U collisions for the spectator centrality  $c_s < 0.1\%$  (left) and  $c_s < 1\%$  (right). In the upper panels the solid lines are the linear fits of our MCG simulation for  $\sigma = 0.7$  fm with the *MB* component for  $\alpha = 0.06$ , and the dashed lines are the same but without the *MB* component for  $\alpha = 0.135$ . The lower panels show the comparison of our results with the STAR data [29] on  $v_2$  in Au+Au collisions at  $\sqrt{s} = 0.2$  TeV and U+U collisions at  $\sqrt{s} = 0.193$  TeV. The solid and dashed lines show the MCG results for  $k\epsilon_2$  with the renormalization constant  $k$  defined to match the experimental  $v_2$  at  $N_{ch} = \langle N_{ch} \rangle$ . The lines have the same meaning as in the upper panels.

has a weak knee-like structure at  $c \sim 1\%$ . The knee for this version is seen better in Fig. 9b, that shows  $\epsilon_2$  versus  $N_{ch}$ . To reduce the statistical fluctuations the curves in Figs. 9a,b have been obtained by averaging of  $\epsilon_2$  in the bins with the width  $\Delta N_{ch} \sim 20$ . For the two versions (with and without the *MB* component) with the fluctuating sources the knee structure in Fig. 9b is absent. Thus we confirm the conclusion of [70] that in the standard MCG wounded nucleon scheme (without the *MB* component) the fluctuations erode the knee structure in  $\epsilon_2$ . This prediction is in contradiction with the analyses [31, 33] where the knee has been found. From Fig. 9a one sees that at small centrality  $\epsilon_2$  without fluctuations of the multiplicity in *pp* collisions becomes smaller by 20–10%. This reduction is considerably bigger than the difference between our two versions with fluctuating sources. Note that at  $c \sim 0.01 - 1\%$  the ratio of our prediction for  $\epsilon_2$  to the flow coefficient  $v_2$  measured by STAR is  $\sim 6 - 6.25$ . It agrees qualitatively with the ratio  $\epsilon_2/v_2$  obtained in hydrodynamical simulations of Refs. [72, 73].

An interesting way to investigate the mechanism of the entropy generation in *AA* collisions and the shape of the initial plasma fireball in collisions of nonspherical nuclei is the use for the centrality categorization signals from the Zero-degree Calorimeters (ZDCs) [74] that detect spectator neutrons. Selecting the events with very low ZDC signals means selection of nearly full-overlap collisions with high multiplicity and very small number of the spectator neutrons [29, 75]. The STAR collaboration [29] have measured the multiplicity dependence of the flow coefficient  $v_2$  for the top 1% and 0.1% most central events selected on the smallness of the ZDC signals in U+U collisions at  $\sqrt{s} = 193$  GeV and in Au+Au collisions at  $\sqrt{s} = 200$  GeV. In the MCG wounded nucleon model the ZDC signal is usually mimicked by the number of the spectator nucleons  $N_s = 2A - N_w$  [71, 75]. However, the equivalence of the centrality categorization via the experimentally measured ZDC activity and that via the  $N_s$  in the MCG simulations is by no means evident. This is because physically it is clear that the dynamical evolution of the hadron systems in the nucleus fragmentation regions after the *AA* collision is a complicated process that can involve interaction of the wounded and not wounded nucleons. These final state interactions, which are completely ignored in the Glauber scheme, can reduce the number of neutrons that could reach the ZDCs. For this reason the possibility to model the ZDCs event selection in terms of  $N_s$  in the MCG simulations should rather be taken as a working hypothesis, to be explored in further studies.

In the present paper we ignore possible dynamical effects in the nucleus fragmentation regions and following previous studies [32, 71] assume that the  $N_s$  categorization reproduces that through the ZDC signals. In terms of the  $N_s$  the

centrality is defined as

$$c_s(N_s) = \sum_{N=0}^{N_s} P_s(N), \quad (28)$$

where  $P_s(N)$  is the probability distribution for  $AA$  collisions in  $N_s$ . The events with very small  $c_s \ll 1$  correspond to collisions with a small impact parameter. For collisions of the nonspherical nuclei the initial asymmetry of the produced fireball is sensitive to angular orientation of the colliding nuclei. For an axis-symmetric nucleus the orientation is described by the pair of the polar angles  $(\theta, \phi)$ . The uranium nucleus has a prolate shape. The high-overlap central tip-tip U+U collisions correspond to the polar angles with  $|\cos \theta_1| + |\cos \theta_2| \approx 2$ . In this case the azimuthal asymmetry of the produced fireball should be dominated by the statistical fluctuations of the nucleon distributions, and should be small. In the case of the highly overlapping body-body collisions with  $|\cos \theta_1| + |\cos \theta_2| \ll 1$  and  $|\phi_1 - \phi_2| \ll \pi$  (or  $|\phi_1 - \phi_2| \approx \pi$ ) the fireball asymmetry should be larger due to the prolate shape of the nucleus ellipsoids. In the MCG simulations the highly overlapping collisions correspond to small values of  $N_s$ . For this reason one can expect that for small  $c_s$  the eccentricity  $\epsilon_2$  should decrease with charged multiplicity  $N_{ch}$ , because the relative contribution of the  $N_{coll}$  term to the entropy production becomes bigger in the tip-tip collisions that give a smaller ellipticity. For Au+Au collisions the situation is opposite to that in U+U collisions, because the gold nucleus has an oblate form. For this reason in the two component Glauber scheme the charged multiplicity in the highly overlapping collisions should be smaller in the tip-tip collisions, and one can expect that for small  $c_s$  the eccentricity  $\epsilon_2$  should grow with the charged multiplicity.

In the upper panels of Fig. 10, we plot the linear fits of our MCG results in the interval  $0.9 < N_{ch}/\langle N_{ch} \rangle < 1.1$  for the rms  $\epsilon_2$  versus the ratio  $N_{ch}/\langle N_{ch} \rangle$  for the spectator centrality windows  $c_s < 0.1\%$  (left) and  $c_s < 1\%$  (right) (the results are shown for the smearing width  $\sigma = 0.7$  fm, but the results for  $\sigma = 0.4$  fm are similar). One sees that, as expected, for the high-overlap collisions in the window  $c_s < 0.1\%$  the slope of the curves is negative for U+U collisions and positive for Au+Au collisions. The slope of the curves is flatter for the version with the  $MB$  component, and for Au+Au collisions this version gives practically flat  $\epsilon_2$ . For  $c_s < 1\%$  the slope of the curves for U+U collisions become a bit lower, but for Au+Au collisions the predictions are very close to that for  $c_s < 0.1\%$ . In the lower panels of Fig. 10 we compare the theoretical predictions with the STAR data [29] on the flow coefficient  $v_2$  for the top 0.1% and 1% ZDC centrality assuming that approximately  $v_2 \approx k\epsilon_2$  [72, 73]. Due to the uncertainties in the value of the ratio  $v_2/\epsilon_2$ , for each case we simply choose the values of  $k$  to match the product  $k\epsilon_2$  to the experimental  $v_2$  at  $N_{ch}/\langle N_{ch} \rangle \approx 1$ . One sees that there is a tendency that the reduction of the slope in the version with the  $MB$  component improves the agreement with the data at the centrality window  $< 0.1\%$ . For U+U collisions in the 1% window the agreement with the data of the results without the  $MB$  component is of similar quality to that with the  $MB$  component. However, there is considerable disagreement with the data for Au+Au collisions. The experimental  $v_2$  has considerable negative slope. The theoretical curve for the version without the  $MB$  component has a small positive slope. The slope becomes positive for the version with the  $MB$  component, but it is much smaller than that for the experimental data. Thus, from Fig. 10 we see that the account of the  $MB$  component improves the agreement with the data (especially for U+U collisions) for the centrality window  $c_s < 0.1\%$ . But for the window  $c_s < 1\%$  the situation is somewhat controversial and one cannot draw a definite conclusion. It is possible that the problem for the window  $c_s < 1\%$  is due to inequivalence of the theoretical centrality categorization via  $N_s$  and that via the ZDC signals used by STAR [29] that may become stronger with increase of centrality.

#### D. p+A and p+p collisions

It is possible that a small size hot QGP may also be produced in  $pA$  and even in  $pp$  collisions. The idea that the QGP may be produced in hadron collisions is very old [76]. The observations of the ridge effect in p+Pb collisions at  $\sqrt{s} = 5.02$  TeV [77–79] and in high multiplicity  $pp$  events at  $\sqrt{s} = 7$  TeV [80] support this idea. The estimates from the observed charged multiplicities show that for the typical  $pPb$  and  $pp$  events at the LHC energies the initial temperature of the mini QGP at the proper time  $\tau \sim 0.5$  fm may be  $\sim 250$  MeV [81, 82], which is well above the deconfinement temperature. In the scenario with the mini QGP formation the ridge effect in  $pPb$  and  $pp$  collisions may be connected with the hydrodynamic expansion of the azimuthally asymmetric initial plasma fireball [83–85].

In this subsection we present our results of the MCG simulation of the mini fireball in  $pPb$  and  $pp$  collisions at  $\sqrt{s} = 5.02$  TeV. As above for Pb+Pb collisions at  $\sqrt{s} = 5.02$  TeV for the parameter  $\alpha$  we use the values obtained from the analysis of the centrality dependence of the charged multiplicity density in Pb+Pb collisions at  $\sqrt{s} = 2.76$  TeV. In Fig. 11 we plot the results for the charged multiplicity density  $dN_{ch}/d\eta$  versus centrality for the versions with and without the meson cloud. As for  $AA$  collisions we define the theoretical centrality through the charged multiplicity distribution at  $\eta = 0$  (18). We compare the results to available data from ALICE [86] obtained via the centrality

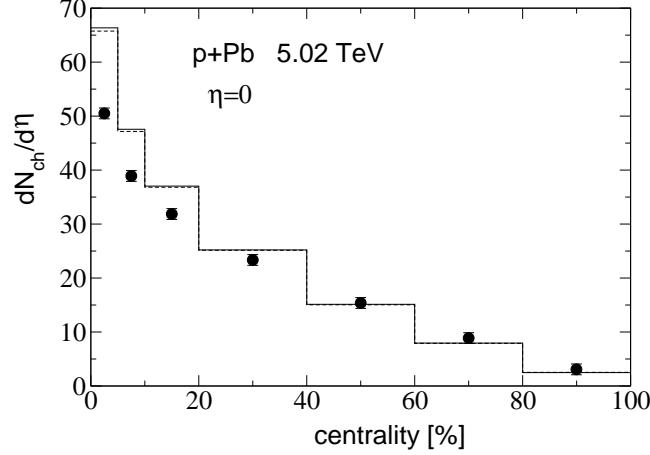


FIG. 11: Centrality dependence of  $dN_{ch}/d\eta$  for p+Pb collisions at  $\sqrt{s} = 5.02$  TeV. Solid: MCG simulation for the scenario with the meson cloud for  $\alpha = 0.09$ . Dashed: MCG simulation without the meson cloud for  $\alpha = 0.14$ . Data are from ALICE [86].

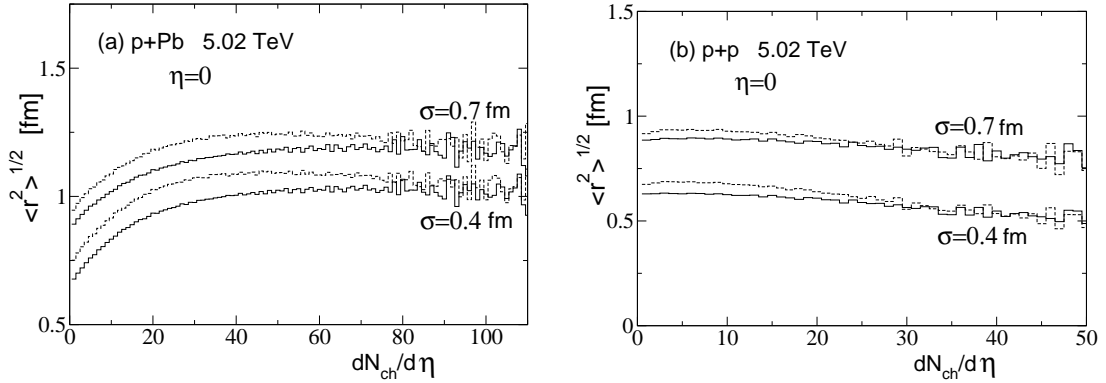


FIG. 12: Multiplicity dependence of  $\langle r^2 \rangle^{1/2}$  for p+Pb (left) and p+p (right) collisions at  $\sqrt{s} = 5.02$  TeV obtained from the MCG simulations for the Gaussian source width  $\sigma = 0.7$  and  $0.4$  fm. Solid: the results for the scenario with the meson cloud for  $\alpha = 0.09$ . Dashed: the results obtained without the meson cloud for  $\alpha = 0.14$ .

estimator corresponding to the central rapidity region (CL1 in Fig. 16 of [86]). Note that the results of [86] obtained via the centrality estimators with large  $|\eta|$  intervals (V0M, V0A in Fig. 16 of [86]) and via the energy deposited in the neutron calorimeter on the Pb-going side (ZNA in Fig. 16 of [86]) give somewhat weaker centrality dependence of the charged multiplicity density. The fact that different centrality estimators give different results are not surprising because for  $pA$  collisions the fluctuations of  $N_{ch}$  at a given impact parameter are of the order of  $N_{ch}$ . For this reason, contrary to  $AA$  collisions where the role of fluctuation turns out to be relatively small [63], the geometry of the  $pA$  collision cannot be accurately determined from the observed charged multiplicity on the event-by-event basis. Despite the above uncertainties with definition of the centrality for  $pA$  collisions, Fig. 11 shows that at a qualitative level the theoretical results agree with the data. A somewhat weaker decrease of the experimental charged multiplicity density with centrality may be due to a considerably wider pseudorapidity region ( $|\eta| < 1.4$ ) used in [86] in the centrality categorization, while our procedure corresponds to  $|\eta| < 0.5$ . It is clear that for a broader  $\eta$  region the effect of the multiplicity fluctuations should be smaller, and the centrality categorization should be biased to the higher centralities. From Fig. 11 one can see that the theoretical results obtained with and without the meson cloud turn out to be very similar. For the mean charged multiplicity density there is no problem with the centrality selection. Our calculations give for the whole centrality window  $dN_{ch}/d\eta \approx 19.5$ , which is in a reasonable agreement with the result  $dN_{ch}/d\eta \approx 17.8$  for all centralities from Ref. [86].

In Fig. 12 we show the results of the MCG simulations with and without the meson cloud for the event-averaged rms radius of the fireball versus the charged multiplicity density for  $pPb$  and  $pp$  collisions at  $\sqrt{s} = 5.02$  TeV obtained for the smearing widths  $\sigma = 0.4$  and  $0.7$  fm. One sees that for moderate charged multiplicities the version with the  $MB$  component gives somewhat smaller fireball radius. It is due to smaller interaction radii in this version. From

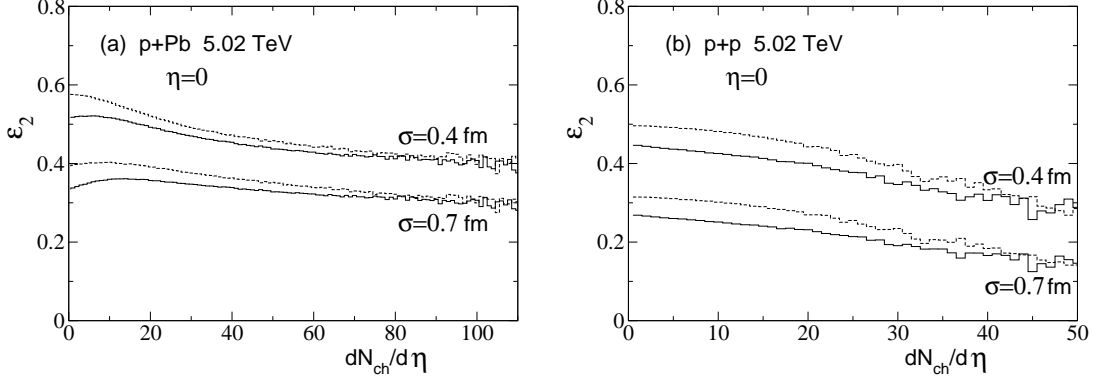


FIG. 13: Multiplicity dependence of the rms  $\epsilon_2$  for p+Pb (left) and p+p (right) collisions at  $\sqrt{s} = 5.02$  TeV obtained from the MCG simulations for the Gaussian source width  $\sigma = 0.7$  and  $0.4$  fm. Solid: the results for the scenario with the meson cloud for  $\alpha = 0.09$ . Dashed: the results for the scenario without the meson cloud for  $\alpha = 0.14$ .

Fig. 12 one can see that the increase of the fireball radius with the smearing width  $\sigma$  is less pronounced for  $pPb$  collisions. This is because for  $pPb$  collisions the geometry of the fireball is largely controlled by the distribution of the nucleons in the nucleus around the path of the projectile proton. The growth of the fireball size with multiplicity for  $pPb$  collisions is connected with the increase of the number of  $NN$  interactions with large impact parameters.

In Fig. 13 we show the results for the multiplicity dependence of the ellipticity  $\epsilon_2$  in  $pPb$  and  $pp$  collisions at  $\sqrt{s} = 5.02$  TeV. One sees that for both  $pPb$  and  $pp$  collisions the ellipticity is smaller for the case with the  $MB$  component. The difference is more pronounced for  $pp$  collisions. The reduction of the ellipticity with the multiplicity for the version without the  $MB$  component is due to the growth of the fraction of the hard component for high multiplicities. It is connected with our choice of the position of the hard sources in the middle between two colliding particles. This mechanism works for the version with the  $MB$  component as well. Of course, the effect should be somewhat weaker due to a smaller value of  $\alpha$ . However, for the case with the  $MB$  component there is an additional mechanism of the reduction of the ellipticity with multiplicity due to the events with simultaneous inelastic interaction of the baryon and meson constituents in the  $MB$  Fock component, that leads to a more symmetric fireball. Note that our results for the rms  $\epsilon_2$  in  $pPb$  collisions for  $\sigma = 0.7$  fm are in a qualitative agreement with the rms flow coefficient  $v_2\{2\} \sim 0.055 - 0.07$  obtained by CMS [77] if one assumes that  $\epsilon_2/v_2 \sim 6$  as was obtained for the large size QGP in the hydrodynamic simulations of Refs. [72, 73]. Unfortunately, the elliptic flow  $v_2$  from CMS [77] is given versus the number of tracks in the CMS detector, and one cannot compare it directly with our  $N_{ch}$  dependence in Fig. 13. But anyway such a comparison could not be conclusive because our theoretical predictions for the geometry of the small size fireball in  $pA$  and  $pp$  collisions depend crucially on the convention for the transverse spacial positions of the entropy sources, and for this reason they are model dependent.

## V. CONCLUSIONS

We have developed a Monte Carlo Glauber model for  $AA$ ,  $pA$  and  $pp$  collisions that accounts for the  $MB$  Fock component of the nucleon. We have used the weight of the  $MB$  component in the nucleon wave function in the IMF that allows one to describe the DIS data on the violation of the Gottfried sum rule [41]. We have found that in the presence of the  $MB$  Fock component the required fraction of the binary collisions in the wounded nucleon model becomes smaller. From the analysis of the STAR data [27] on the charged multiplicity density in Au+Au collisions at  $\sqrt{s} = 0.2$  TeV we obtained the fraction of the binary collisions  $\alpha = 0.06$  and  $0.135$  for the versions with and without the  $MB$  component, respectively. A similar fit to the ALICE data [52] on Pb+Pb collisions at  $\sqrt{s} = 0.2$  TeV gives for the two versions  $\alpha = 0.09$  and  $0.14$ . Our results show that for central  $AA$  collisions at the RHIC and LHC energies the meson cloud can increase the multiplicity density in the central rapidity region by  $\sim 16 - 18\%$ . We have found that the  $MB$  component leads to the growth of the ratio the charged multiplicity density to the number of the wounded nucleons from peripheral to central  $AA$  collisions by  $\sim 20\%$  and  $\sim 15\%$  at RHIC and LHC energies, respectively.

We have used the results of our fit to the data on the charged multiplicity density in Pb+Pb collisions at  $\sqrt{s} = 2.76$  TeV to give predictions for the future LHC run 2 at  $\sqrt{s} = 5.02$  TeV. As compared to  $\sqrt{s} = 2.76$  TeV we have found the growth of  $dN_{ch}/d\eta$  in the central Pb+Pb collisions for  $\sqrt{s} = 5.02$  TeV by about  $20\%$ .

We have found that the effect of the meson cloud on the eccentricity  $\epsilon_2$  in Au+Au and Pb+Pb collisions is relatively small, except for very peripheral collisions, where it reduces  $\epsilon_2$  by  $\sim 20\%$ . We have also studied the eccentricity  $\epsilon_2$

for collisions of the deformed uranium nuclei. For U+U collisions our MCG simulations with and without the  $MB$  component give  $\epsilon_2$ , that has not a knee-like structure in the top central collisions. Our results for  $\epsilon_2$  for the version without the  $MB$  component are in contradiction with the results of Refs. [31, 33] that predicted the knee-like structure in  $\epsilon_2$ . We find the knee structure only for the version of the MCG model without the meson cloud and without multiplicity fluctuations in  $pp$  collisions. This is in agreement with the results of the analyses [30, 70]. We have also studied the multiplicity dependence of  $\epsilon_2$  for the top central U+U and Au+Au collisions with the centrality  $c_s$  defined via the number of the spectator nucleons  $N_s$  that is used to model the centrality categorization via the ZDC signals [74]. We have found that for  $c_s < 0.1\%$  the  $MB$  Fock component improves the agreement with the STAR data [29] on the  $N_{ch}$  dependence of  $\epsilon_2$ . But the results for  $c_s < 1\%$  disagree with the data (especially for Au+Au collisions). It is possible that it is due to inequivalence of the theoretical centrality categorization via  $N_s$  and that via the ZDC signals used by STAR [29].

We have also applied our MCG model to  $pA$  and  $pp$  collisions. We have found that the effect of the  $MB$  component may be more important for the initial asymmetry of the plasma fireball in  $pA$  and  $pp$  collisions, where it gives reduction of the eccentricity  $\epsilon_2$  by  $\sim 15 - 20\%$  for the typical charged multiplicities. We have found that for the small size fireball produced in  $pA$  and  $pp$  collisions the MCG model with the meson cloud reduces the size of the fireball by  $10 - 20\%$ .

Because the  $MB$  components are the long-range fluctuations in the physical nucleon, one can expect that the observed effects should exist in other schemes of the entropy production. For this reason it would be of great interest to study the effect of the meson cloud within the IP-Glasma model [5, 6] (especially for  $pA$  and  $pp$  collisions, where the effect of the  $MB$  component should be bigger).

### Acknowledgments

I thank W. Broniowski and S.A. Voloshin for communications. This work is supported in part by the grant RFBR 15-02-00668-a.

### References

- 
- [1] P. Huovinen, Int. J. Mod. Phys. E**22**, 1330029 (2013) [arXiv:1311.1849], and references therein.
  - [2] R.Derradi de Souza, T. Koide, and T. Kodama, Prog. Part. Nucl. Phys. **86**, 35 (2016) [arXiv:1506.03863], and references therein.
  - [3] U. Heinz and R. Snellings, Ann. Rev. Nucl. Part. Sci. **63**, 123 (2013) [arXiv:1301.2826].
  - [4] H. Song, S.A. Bass, U. Heinz, and T. Hirano, Phys. Rev. C**83**, 054910 (2011), Erratum: Phys. Rev. C**86**, 059903 (2012) [arXiv:1101.4638].
  - [5] B. Schenke, P. Tribedy, and R. Venugopalan, Phys. Rev. Lett. **108**, 252301 (2012) [arXiv:1202.6646].
  - [6] B. Schenke, P. Tribedy, and R. Venugopalan, Phys. Rev. C**86**, 034908 (2012) [arXiv:1206.6805].
  - [7] A. Bialas, M. Bleszynski, and W. Czyz, Nucl. Phys. B**111**, 461 (1976).
  - [8] D. Kharzeev and M. Nardi, Phys. Lett. B**507**, 121 (2001) [nucl-th/0012025].
  - [9] L.D. McLerran and R. Venugopalan, Phys. Rev. D**49**, 2233 (1994) [hep-ph/9309289].
  - [10] N.N. Nikolaev and B.G. Zakharov, Z. Phys. C**49**, 607 (1991); *ibid.*, C**53**, 331 (1992).
  - [11] V. Barone, M. Genovese, N.N. Nikolaev, E. Predazzi, and B.G. Zakharov, Z. Phys. C**58**, 541 (1993).
  - [12] N.N. Nikolaev and B.G. Zakharov, Phys. Lett. B**332**, 184 (1994) [hep-ph/9403243].
  - [13] F.E. Low, Phys. Rev. D**12**, 163 (1975).
  - [14] E.V. Shuryak, Rev. Mod. Phys. **65**, 1 (1993).
  - [15] A. Casher, H. Neuberger, and S. Nussinov, Phys. Rev. D**20**, 179 (1979).
  - [16] E. Gotsman and S. Nussinov, Phys. Rev. D**22**, 624 (1980).
  - [17] N.N. Nikolaev, B.G. Zakharov, and V.R. Zoller, JETP Lett. **59**, 6 (1994) [hep-ph/9312268].
  - [18] N.N. Nikolaev and B.G. Zakharov, Phys. Lett. B**327**, 149 (1994) [hep-ph/9402209].
  - [19] R. Fiore, N.N. Nikolaev, and V.R. Zoller, JETP Lett. **99**, 363 (2014) [arXiv:1403.1950].
  - [20] A. Bialas and M. Jezabek, Phys. Lett. B**590**, 233 (2004) [hep-ph/0403254].
  - [21] A. Bialas, A. Bzdak, and R. Peschanski, Phys. Lett. B**665**, 35 (2008) [arXiv:0804.2364].
  - [22] A. Bzdak, Acta Phys. Polon. B**41**, 2471 (2010) [arXiv:0906.2858].
  - [23] B. Alver, M. Baker, C. Loizides, and P. Steinberg, arXiv:0805.4411.
  - [24] W. Broniowski, M. Rybczynski, and P. Bozek, Comput. Phys. Commun. **180**, 69 (2009) [arXiv:0710.5731].



- [25] M. Rybczynski, G. Stefanek, W. Broniowski, and P. Bozek, *Comput. Phys. Commun.* **185**, 1759 (2014) [arXiv:1310.5475].
- [26] B.B. Back *et al.* [PHOBOS Collaboration], *Phys. Rev.* **C70**, 021902 (2004) [nucl-ex/0405027].
- [27] B.I. Abelev *et al.* [STAR Collaboration], *Phys. Rev.* **C79**, 034909 (2009) [arXiv:0808.2041].
- [28] M. Rybczynski, W. Broniowski, arXiv:1510.08242.
- [29] L. Adamczyk *et al.* [STAR Collaboration], *Phys. Rev. Lett.* **115**, 222301 (2015) [arXiv:1505.07812].
- [30] P. Filip, R. Lednicky, H. Masui, and N. Xu, *Phys. Rev.* **C80**, 054903 (2009).
- [31] S.A. Voloshin, *Phys. Rev. Lett.* **105**, 172301 (2010) [arXiv:1006.1020].
- [32] J.S. Moreland, J.E. Bernhard, and S.A. Bass, *Phys. Rev.* **C92**, 011901 (2015) [arXiv:1412.4708].
- [33] S. Chatterjee *et al.*, *Phys. Lett.* **B758**, 269 (2016) [arXiv:1510.01311].
- [34] A. Bialas, W. Czyz, and W. Furmanski, *Acta Phys. Polon.* **B8**, 585 (1977).
- [35] A. Bialas and W. Czyz, *Acta Phys. Polon.* **B10**, 831 (1979).
- [36] P. Bozek, W. Broniowski, and M. Rybczynski, arXiv:1604.07697.
- [37] A. Bialas and A. Bzdak, *Phys. Rev.* **C77**, 034908 (2008) [arXiv:0707.3720].
- [38] S. Eremín and S. Voloshin, *Phys. Rev.* **C67**, 064905 (2003) [nucl-th/0302071].
- [39] C. Loizides, arXiv:1603.07375.
- [40] S.S. Adler *et al.* [PHENIX Collaboration], *Phys. Rev.* **C89**, 044905 (2014) [arXiv:1312.6676].
- [41] J. Speth and A.W. Thomas, *Adv. Nucl. Phys.* **24**, 83 (1997).
- [42] S.D. Drell and K. Hiida, *Phys. Rev. Lett.* **7**, 199 (1961).
- [43] R.T. Deck, *Phys. Rev. Lett.* **13**, 169 (1964).
- [44] A.B. Kaidalov, *Phys. Rept.* **50**, 157 (1979).
- [45] M.L. Good and W.D. Walker, *Phys. Rev.* **120**, 1857 (1960).
- [46] K.G. Boreskov, A.B. Kaidalov, and L.A. Ponomarev, *Yad. Fiz.* **17**, 1285 (1973); **19**, 1103 (1974).
- [47] K.G. Boreskov, A.A. Grigorian, and A.B. Kaidalov, *Sov. J. Nucl. Phys.* **24**, 411 (1976) 411.
- [48] B.G. Zakharov and V.N. Sergeev, *Sov. J. Nucl. Phys.* **38**, 947 (1983).
- [49] B.G. Zakharov and V.N. Sergeev, *Yad. Fiz.* **28**, 1339 (1978).
- [50] V.N. Gribov, *Sov. Phys. JETP* **29**, 483 (1969).
- [51] A. Kaidalov, *Nucl. Phys.* **A525**, 39 (1991).
- [52] K. Aamodt *et al.* [ALICE Collaboration], *Phys. Rev. Lett.* **106**, 032301 (2011) [arXiv:1012.1657].
- [53] B.G. Zakharov, *JETP Lett.* **104**, 6 (2016) [arXiv:1605.06012].
- [54] V.R. Zoller, *Z. Phys.* **C60**, 141 (1993).
- [55] V.R. Zoller, *Z. Phys.* **C53**, 443 (1992).
- [56] W. Melnitchouk, J. Speth, and A.W. Thomas, *Phys. Rev.* **D59**, 014033 (1998) [hep-ph/9806255].
- [57] H. Holtmann, A. Szczurek, and J. Speth, *Nucl. Phys.* **A596**, 631 (1996) [hep-ph/9601388].
- [58] J.D. Sullivan, *Phys. Rev.* **D5**, 1732 (1972).
- [59] A. Szczurek and J. Speth, *Nucl. Phys.* **A555**, 249 (1993).
- [60] A.B. Kaidalov and M.G. Poghosyan, *Eur. Phys. J.* **C67**, 397 (2010) [arXiv:0910.2050].
- [61] A. Capella and E.G. Ferreira, *Eur. Phys. J.* **C72**, 1936 (2012) [arXiv:1110.6839].
- [62] B. Müller and K. Rajagopal, *Eur. Phys. J.* **C43**, 15 (2005) [hep-ph/0502174].
- [63] W. Broniowski and W. Florkowski, *Phys. Rev.* **C65**, 024905 (2002) [nucl-th/0110020].
- [64] D. Teaney and L. Yan, *Phys. Rev.* **C83**, 064904 (2011) [arXiv:1010.1876].
- [65] E. Retinskaya, M. Luzum, J.-Y. Ollitrault, *Nucl. Phys.* **A926**, 152 (2014) [arXiv:1401.3241].
- [66] C. Albajar *et al.* [UA1 Collaboration], *Nucl. Phys.* **B335**, 261 (1990).
- [67] J. Adam *et al.* [ALICE Collaboration] arXiv:1509.07541.
- [68] B. Abelev *et al.* [ALICE Collaboration], *Eur. Phys. J.* **C73**, 2456 (2013) [arXiv:1208.4968].
- [69] R.E. Ansorge *et al.* [UA5 Collaboration] *Z. Phys.* **C43**, 357 (1989).
- [70] M. Rybczynski, W. Broniowski, and G. Stefanek, *Phys. Rev.* **C87**, 044908 (2013) [arXiv:1211.2537].
- [71] A. Goldschmidt, Z. Qiu, C. Shen, and U. Heinz, arXiv:1502.00603.
- [72] H. Niemi, G.S. Denicol, H. Holopainen, and P. Huovinen, *Phys. Rev.* **C87**, 054901 (2013) [arXiv:1212.1008].
- [73] Z. Qiu and U.W. Heinz, *Phys. Rev.* **C84**, 024911 (2011) [arXiv:1104.0650].
- [74] A. Goldschmidt, Z. Qiu, C. Shen, and U. Heinz, *Phys. Rev.* **C92**, 044903 (2015) [arXiv:1507.03910].
- [75] A.J. Kuhlman and U.W. Heinz, *Phys. Rev.* **C72**, 037901 (2005) [nucl-th/0506088].
- [76] E.V. Shuryak, *Phys. Lett.* **B78**, 150 (1978).
- [77] S. Chatrchyan *et al.* [CMS Collaboration], *Phys. Lett.* **B718**, 795 (2013) [arXiv:1210.5482].
- [78] B. Abelev *et al.* [ALICE Collaboration], *Phys. Lett.* **B719**, 29 (2013) [arXiv:1212.2001].
- [79] G. Aad *et al.* [ATLAS Collaboration], *Phys. Rev. Lett.* **110**, 182302 (2013) [arXiv:1212.5198].
- [80] S. Chatrchyan *et al.* [CMS Collaboration], *JHEP* **1009**, 091 (2010) [arXiv:1009.4122].
- [81] B.G. Zakharov, *Phys. Rev. Lett.* **112**, 032301 (2014) [arXiv:1307.3674].
- [82] B.G. Zakharov, *J. Phys.* **G41**, 075008 (2014) [arXiv:1311.1159].
- [83] W. Broniowski, P. Bozek, M. Rybczynski, and E.R. Arriola, *Acta Phys. Polon. Supp.* **8**, 301 (2015) [arXiv:1506.04362].
- [84] P. Bozek, *Acta Phys. Polon.* **B41**, 837 (2010) 837 [arXiv:0911.2392].
- [85] M. Habich, G.A. Miller, and P. Romatschke, *Eur. Phys. J.* **C76**, 408 (2016) [arXiv:1512.05354].
- [86] J. Adam *et al.* [ALICE Collaboration], *Phys. Rev.* **C91**, 064905 (2015) [arXiv:1412.6828].